Chin. Geogra. Sci. 2022 Vol. 32 No. 5 pp. 808−823
https://doi.org/10.1007/s11769-022-1302-4

Springer Science Press
www.springerlink.com/content/1002-0063

Ecological Risk Assessment of World Heritage Sites Using RS and GIS: A Case Study of Huangshan Mountain, China

HUANG Shiman[1], HU Qingwu[1], WANG Shaohua[1], LI Haidong[2]

(1. *School of Remote Sensing and Information Engineering*, *Wuhan University*, *Wuhan* 430079, *China*; 2. *Nanjing Institute of Environmental Sciences*, *Ministry of Ecology and Environment*, *Nanjing* 210042, *China*)

Abstract: Ecological risk assessment (ERA) is an indispensable method for systematic monitoring of World Heritage Sites (WHSs) exposed to various anthropogenic factors and natural disasters. Remote sensing (RS) and geographical information systems (GIS) can eliminate many limitations in traditional ERA methods. In this study, changes in ecological risk at Huangshan Mountain, the first mixed WHS in China, over the period of 1984–2019 were explored using remote sensing images and products by considering both natural disasters and human disturbance. Results show that of the four land cover types in Huangshan Mountain, namely water, forest, building and farmland, the main land cover type is forest. During the 35 yr, lands categorised at low or relatively low ecological risk levels are dominant in Huangshan Mountain, with the lowest and highest *ERI*s (ecological risk index) in 1990 and 2010, respectively. The areas at the five ecological risk levels have declined as follows: relatively low > low > medium > relatively high > high. Changes in ecological risks are closely related to changes in land cover and natural disasters. Even though major natural disasters may affect the ecological risk level in the whole region, changes in land cover caused by human activities will shift the ecological risk level in some areas. Our attempts can be modified and applied to other sites, and offer policy implications for protection and preservation of WHSs.

Keywords: ecological risk assessment; ecological risk index (*ERI*); world heritage site; landscape ecological index; Huangshan Mountain; Remote Sensing

Citation: HUANG Shiman, HU Qingwu, WANG Shaohua, LI Haidong, 2022. Ecological Risk Assessment of World Heritage Sites Using RS and GIS: A Case Study of Huangshan Mountain, China. *Chinese Geographical Science*, 32(5): 808−823. https://doi.org/10.1007/s11769-022-1302-4

1 Introduction

World Heritage Sites (WHSs) designated by the United Nations Educational Scientific and Culture Organization (UNESCO) are aimed at conserving the sites of outstanding cultural or natural heritage for future generations (UNESCO, 2019). To be selected as a WHS, a landmark must be unique to some extent, which means it must be identified geographically or historically and has special cultural or material significance. There are three types of sites: cultural, natural, and mixed, with mixed meaning containing elements of both natural and cultural significance. As of January 2021, there are 1121 WHSs (869 cultural, 213 natural, and 39 mixed) in 167 countries. China has 55 WHS (37 cultural, 14 natural, and 4 mixed), making it one of the countries with the most WHSs. Unfortunately, WHSs are vulnerable to diverse anthropogenic factors and natural disasters, such

Received date: 2021-09-08; accepted date: 2022-01-16
Foundation item: Under the auspices of the National Key Research and Development Program of China (No. 2020YFC1521903), National Key Research and Development Program of China (No. 2018YFD1100104)
Corresponding author: HU Qingwu. E-mail: huqw@whu.edu.cn

as urbanisation, erosion, and landslides (Alexakis et al., 2013; Agapiou et al., 2015; Agapiou et al., 2016; Murray et al., 2018). For example, the Buddhas of Bamiyan in Afghanistan were blown up and destroyed by the Taliban in March 2001 (Crippa et al., 2013); many cave temple heritages were severely damaged in the 2008 Wenchuan Earthquake in China (Isceah et al., 2010); and the Hiraizumi cultural heritages of the Ogasawara Islands and Iwate Prefecture were destroyed in the 2011 Japanese tsunami (Sugio, 2015). To ensure the long-term sustainability of WHSs and encourage remedial action, the Convention of World Heritage has constructed a 'List of World Heritage in Danger' to identify the sites that are at risk of serious and specific dangers (Ryan and Silvanto, 2009). To preserve WHSs, risk preparedness and prevention are regarded as the best measures (Agapiou et al., 2015; Levin et al., 2019). The 'Convention for the Protection of World Cultural and Natural Heritage' states that WHSs entail periodical professional inspections, reviews and evaluations. The recognition of these issues has boosted studies on WHS risk management (Accardo et al., 2003; Mecocci et al., 2014; Hong et al., 2015).

Ecological risk assessment (ERA) is an evaluation process to assess the likelihood of adverse environmental impacts from one or more external factors, through which preventive conservation measures can be adopted to reduce risks and promote the sustainable development of WHSs (Norton et al., 1992; Alexakis and Sarris, 2010). Nowadays, risk maps are regarded as an essential part of the ERA process because they contain information on the spatial distribution of natural phenomena, environmental elements and certain human activities (Bathrellos et al., 2017; Lyu et al., 2018; Skilodimou et al., 2019). Traditionally, an ERA requires large amounts of data and information, including from field surveys, some of which are time-consuming and costly and sometimes even impossible to collect, as there is often not enough suitable equipment and tools to carry out the necessary collections. As a result, many attempts to quantify the ecological risk have been limited due to a lack of data (Joppa et al., 2016). Over the last two decades, remote sensing (RS) has shown great potentials as an essential tool for ERA to provide ecologically relevant long-term datasets. With robust spatial analysis and information integration capabilities, GIS supports the straightforward exploration of various data types, especially in assessing diverse natural disasters and land cover planning (Murray et al., 2018). By combining RS with GIS, ERA has been successfully implemented in a reliable, repetitive, rapid and cost-effective way based mainly on spatial information of WHSs (Alexakis and Sarris, 2010; Agapiou et al., 2015; Liu et al., 2019). Furthermore, multi-period data can facilitate dynamic monitoring (Liu and Li, 2018; Zhang et al., 2018). However, most existing research has focused on the detailed examination of a single hazard phenomenon. In fact, in most cases, an area is not affected by only one natural hazard but by two or more natural ones. As a result, using one hazard map for each type of natural hazard becomes challenging to manage. Therefore, multi-hazard analyses should be conducted (Alexakis and Sarris, 2010; Agapiou et al., 2016; Skilodimou et al., 2019).

Various approaches have been developed for natural hazard estimation, such as heuristic approaches based on expert judgment (Aleotti and Chowdhury, 1999), statistical techniques (Papadopoulou-Vrynioti et al., 2013), and fuzzy logic approaches (Assimakopoulos et al., 2003). Significantly, the analytical hierarchy process (AHP), one of the most popular techniques proposed by Satty in the 1970s, is a multi-criteria decision-making method based on the pairwise comparison, which is constructed by combining qualitative and quantitative factors to rank the alternatives. In addition, combined with GIS, this method has been successfully implemented in single hazard assessments (Siddayao et al., 2014; Ghosh and Kar, 2018) and multi-hazard assessments (Agapiou et al., 2016; Bathrellos et al., 2017). For example, Bathrellos et al. (2017) have integrated GIS and AHP to pinpoint suitable areas for urban development.

However, with the increasingly heavy impact of human activities on the ecological environment, previous studies on natural hazards are no longer appropriate, especially for WHSs. Although some researchers have considered human activities (Yan and Morrison, 2008; Agapiou et al., 2015), the indicators presented in their studies usually rely on questionnaire data and government statistics. Later, a type of ERA focusing on landscape ecology has emerged as an essential branch of ERA. Firstly proposed by Turner et al. (2001), the landscape is defined as a scale of human economic activity, and landscape ecology highlights the interaction among

spatial patterns, ecological processes, and scales. So far, the landscape has become an appropriate scale to explore the ways and degrees of ecological impacts of human activities. Based on landscape patterns, ERA can comprehensively evaluate numerous possible human impacts and their cumulative consequences, and many studies have been carried out in this field (Zhang and Xie, 2015; Li et al., 2017; Liu and Li, 2018; Zhang et al., 2018; Zhang et al., 2020). This study will adopt the landscape index to measure a specific area's landscape patterns and human disturbances.

In this study, Huangshan Mountain, is selected as the study site. As one of China's most famous tourist destinations, Huangshan Mountain has been recognized as 'the loveliest mountain of China', and in 1990 UNESCO listed it as a mixed WHS, the first in China. Since then, the tourism industry has developed rapidly, and the number of tourists has significantly increased. In 1979, the number of tourists to Huangshan Mountain was only 104 292 (Huang, 1992); but in 2019, the number soared to 3 501 000 (Wang et al., 2021). However, along with rapid economic and social development, the ecological environmental pressure on Huangshan Mountain goes up seriously. Although many studies have been conducted on tourism resources, water resources and ecological function zoning of Huangshan Mountain, few have assessed its overall ecological risk (Liang, 1993; Guan et al., 2005; Gong et al., 2009; Wang et al., 2014; Ma et al., 2019).

Therefore, this study aimed to: 1) develop a multi-hazard model to describe its natural hazards; 2) adopt a landscape index to quantify the interference of human activities; and 3) assess the ecological risk and identify the spatiotemporal dynamic variations in Huangshan Mountain.

2 Materials and Methods

2.1 Study area

Huangshan Mountain is located in Huangshan City in the south of Anhui Province in China, with a total area of approximately 1200 km^2, 40 km long from north to south and 30 km wide from east to west. In 1990, Huangshan Mountain was listed as a mixed WHS; in 2004, it was further selected as a World Geopark; and in 2007, it was selected as a National Grade 5A tourist attraction. Famous for its magnificent natural sceneries and rich plant resources, Huangshan Mountain plays a crucial role in protecting many local or national plant species, some of which are endangered. The present case study covers the Scenic Area of Huangshan Mountain, with a total area of 160.6 km^2, ranging from 30°01′N to 30°18′N and from 118°01′E to 118°17′E (Fig. 1).

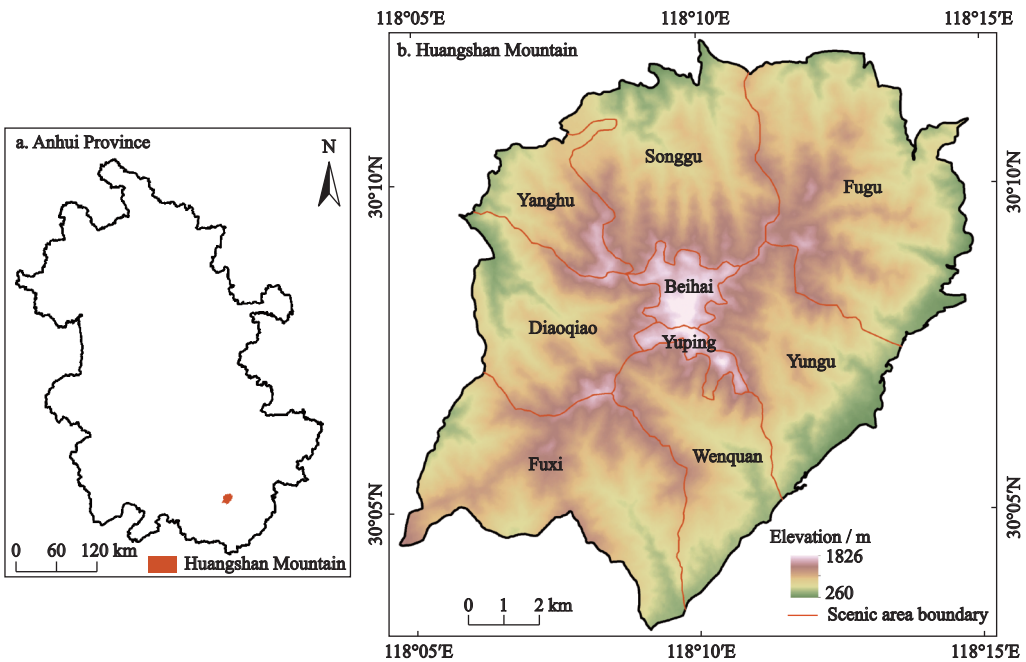

Fig. 1 Location of Huangshan Mountain, China

Sprawling along the middle and lower reaches of the Yangtze River, Huangshan Mountain has a subtropical monsoon climate, with an average temperature of 7.9°C. Its local topography of high mountains and deep valleys plays a leading role in its climates and climate changes in the vertical direction. The average annual precipitation of Huangshan Mountain is 2394.5 mm, with 181 precipitation days annually on average. Precipitation is generally concentrated in the spring and summer of each year. These two seasons account for approximately 60% of the annual precipitation, making the region prone to flood disasters and soil erosion. However, the lack of rains in the summer months can easily cause water shortages in the mountains, thus forming 'summer droughts' (Yang, 2014). The average elevation of the scenic area is approximately 1600 m, with 77 peaks above 1000 m, among which the highest is Lianhua Peak, reaching up to 1864.8 m.

2.2 Data sources and processing

The satellite images used in this study are obtained from the United States Geological Survey (http://earthexplrer.usgs.gov/). According to the availability of cloudless datasets during the vegetation growth periods, images mainly during summer months are retrieved. In this study, Landsat 5 Thematic Mapper (TM) images (30 m) at Oct. 30, 1984, Aug. 28, 1990, Jul. 22, 2000, and Oct. 8, 2010, and Landsat 8 Operational Land Imager (OLI) images (30 m) at Oct. 31, 2019 are selected. The digital elevation model (DEM) of Huangshan Mountain, with a 30 m pixel size, is downloaded from the Geospatial Data Cloud website (http://www.gscloud.cn). All the image datasets are first georeferenced into a standard geodetic system (WGS1984, UTM Zone 50N). The Landsat image pre-processing was performed with ENVI 5.3, including atmospheric correction, radiation calibration and image cropping. Auxiliary data include the precipitation data at Guangming Peak from 1984 to 2019 and the district map of Huangshan Mountain.

The maximum likelihood method, a supervised classification method, is adopted for image classification in ENVI 5.3. Both the training and the test samples for each land cover type are selected via visual interpretation and Google Earth samples. The training samples are used to train the judgment function, which will then be used to classify other data that need to be classified. After the image classification, the test samples will be used to test the image classification accuracy. According to China's National Standard for Land Use Classification (GB/T 21010−2017) (Ministry of Land and Resources of the People's Republic of China, 2017) and the current conditions of Huangshan Mountain, four types of land cover have been identified, namely, water, forest, building, and farmland. For classification accuracy, the kappa coefficient and the overall accuracy of each classified image are both within the acceptable ranges for further analyses: the former is over 0.8, and the latter is approximately 87%.

2.3 Methods

Risk is defined as the product of the probability of risk occurrence and its consequence in a specific area and period (Hunsaker et al., 1990; Fu and Xu, 2001; Liu and Li, 2018). The overall method of this study is presented in Fig. 2. Data processing software adopted include ENVI 5.3, ArcGIS 10.5 and Fragstats4.2.

2.3.1 Pre-processing

An essential feature of ERA is the spatial heterogeneity of risk receptors and risks in the study area. In order to spatialize the ecological risks and enhance the accuracy of ERA, it is necessary to divide the study area into different risk cells (Zhang and Xie, 2015; Li et al., 2017; Liu and Li, 2018). In this study, the equidistant system sampling method are used to obtain square grids with sides length of 500 m.

After risk cell division, the risks and risk receptors of the case study area are defined. In landscape ecological risk assessments, risk receptors usually consist of multiple types of ecosystems rather than one single element, and different kinds of ecosystems play different roles in the overall ecological function of a region. In this study, the ecosystems represented by the above four kinds of land cover are taken as risk receptors. According to UNESCO, the ecological risks of Huangshan Mountain include storm damage to trees, landslides, water shortages that increase fire hazards, erosion, pressure from visitors, and pinewood nematode pests. We selected several significant risks based on previous researches, namely, droughts, erosions, and geological disasters.

Each risk cell corresponds to different risks and risk receptors. Each risk cell's risk probability is evaluated by combining the assessment maps for droughts, erosions and geological disasters, and a landscape ecological index is introduced to assess its vulnerability.

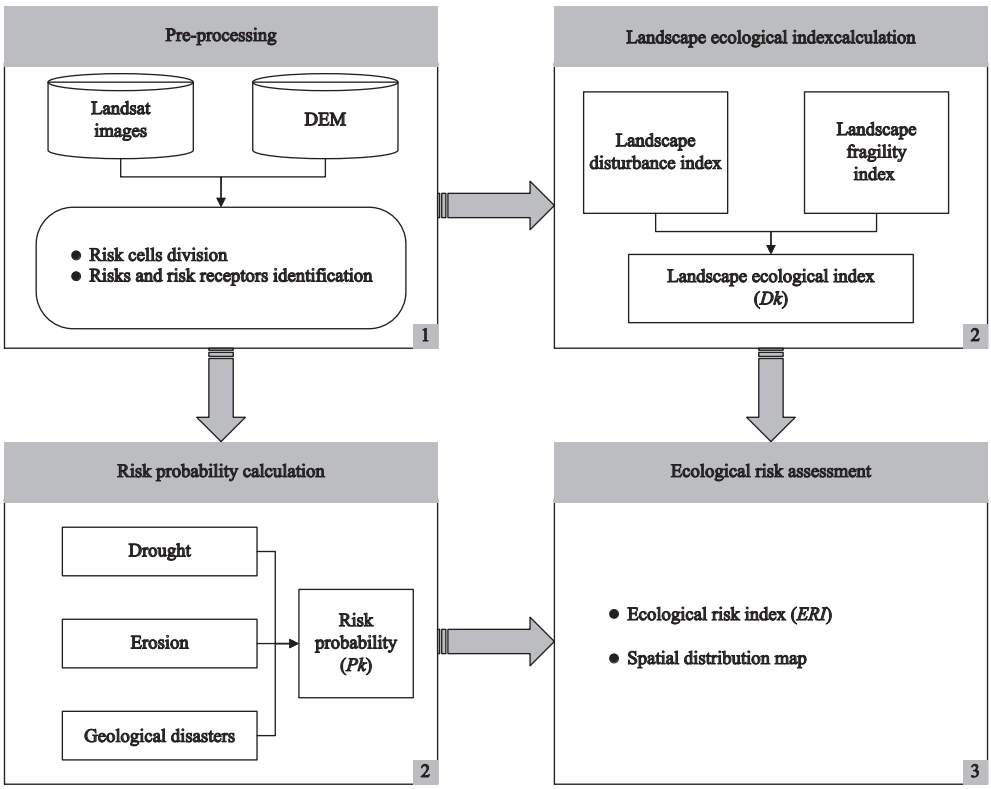

Fig. 2 Framework of this study. DEM is digital elevation model

Then, the ecological risk of each risk cell is obtained and used as the centroid value of a given risk cell to spatially interpolate the ecological risk map.

2.3.2 Risk probability calculation

After identifying risks, the necessary remote sensing data are collected for further analyses in the GIS to determine the risk probability of natural hazards.

(1) Drought

Due to the influence of high altitudes, Huangshan Mountain is highly vulnerable to the monsoon climate. Although the average annual precipitation is massively abundant, the seasonal distribution of the precipitation is particularly uneven due to the seasonality of the atmospheric circulation. Additionally, due to a large amount of runoff, the drainage is good in the rainy seasons, but the water storage capacity of the mountain is weak in the less rainy seasons. Therefore, seasonal droughts often occur in Huangshan Mountain (Cheng, 2010). Using land surface temperature (*LST*) and normalized difference vegetation index (*NDVI*) alone for drought monitoring is one-sided. Instead, integrated analysis based on the two-dimensional feature space of *NDVI-LST* is a more common technique (Sandlot et al., 2002; Zhang et al., 2007; Belal et al., 2014; Du et al., 2017; Ali et al., 2019). Sandlot et al. (2002) simplified the *NDVI-LST* two-dimensional feature space into a triangle and proposed a temperature vegetation dryness index (*TVDI*), as expressed in Eq. (1):

$$TDVI = (T_s - T_{smin}) / T_{smax} - T_{smin} \quad (1)$$

where T_s represents the *LST*; and T_{smin} and T_{smax} represent the minimum and maximum *LST*, respectively, of pixels with the same *NDVI* value in the image. The *TVDI* values range from 0 to 1 and are classified into five categories according to Zhang et al. (2007).

(2) Erosion

Among various factors that affect soil erosions, terrain slope, land cover type, and vegetation coverage deliver the most significant effects (Pandey et al., 2009; Zhou and Feng, 2018). According to the classification standard for soil erosions issued by the Ministry of Water Resources of China (Ministry of Water Resources of the People's Republic of China, 2008), Huangshan Mountain shall be regarded as a water erosion area. The land cover type, vegetation coverage and slope can be used as the criteria for water erosions to analyze the erosion intensity in Huangshan Mountain, as shown in Table 1.

Table 1 Erosion intensity classification for different land cover types in Huangshan Mountain, China

Land cover types	Vegetation coverage / %	Slope / °					
		< 5	5–8	8–15	15–25	25–35	> 35
Forest	60–75	Low	Low	Low	Low	Medium	Medium
	45–60	Low	Low	Low	Medium	Medium	High
	30–45	Low	Low	Medium	Medium	High	Very high
	< 30	Low	Medium	Medium	High	Very high	Severe
Farmland	−	Low	Low	Medium	Medium	High	Very high
Water	−	Low	Low	Low	Low	Low	Low
Building	−	Low	Low	Low	Low	Low	Low

Note: − means no data

(3) Geological disasters

Heavy amounts and strong intensities characterize the precipitation on Huangshan Mountain. A large amount of precipitation may cause sharp mountain torrents, easily triggering geological disasters, such as mudslides and landslides. Based on the existing researches, 10 indicators are selected to establish an evaluation system for the probability of geological disasters (Kayastha et al., 2013; Agapiou et al., 2015; Bathrellos et al., 2017; Lyu et al., 2018; Zang et al., 2018; Skilodimou et al., 2019). Among the 10 indicators, slope, elevation, aspect, curvature, relative relief, vegetation coverage, river proximity, and river density are hazard-forming factors, while precipitation and precipitation days in the rainy seasons are hazard-inducing factors. The stages of the approach consist of: 1) factor extraction and rating. All factors extracted from primary remote sensing data are divided into classes representing different stability conditions. Each class is standardized to a unified rating scale, with a value range from 1 to 5. The greater the value, the more favorable the conditions are for geological disasters. 2) Weight determination: AHP is applied to compare the relative importance of different factors and calculate the criterion weights. After the hierarchy order is determined, a pairwise comparison matrix is constructed based on the relative importance of each factor to the others. In this matrix, the value is ranged from 1 for 'equal importance' to 9 for 'extreme importance'. Then, the matrix is normalized by dividing each column with the corresponding sum. Finally, the weight of each factor is obtained by calculating the average of each row. Yaahp software is used to construct the matrix and calculate the weights in this study. The relative importance is then acquired from references (Kayastha et al., 2013; Lyu et al., 2018; Zang et al., 2018). 3) Overall analysis: The weighted linear combination is implemented to generate the final distribution map, which is then further classified, based on natural breaks in the cumulative frequency histogram, into five classes: i) very low; ii) low; iii) medium; iv) high, and v) very high.

(4) Multi-hazard map

As mentioned above, the hazard maps for droughts, erosions and geological disasters in the study area are classified into five categories. However, the simple integration of three hazard maps is insufficient to produce a reliable multi-hazard map. Many existing researches have implemented AHP to determine the weight values for their entire study areas, but the time span of this study is 35 yr, meaning that the main risk factors would have changed over different periods, so it is not reasonable to maintain consistent weight values over time.

To address the problem, this study puts the hazard maps mentioned above into the risk cells. The product of the proportion of its distribution area in a risk cell and the risk intensity level is then used as the risk weight for that cell. In this way, the same risk does not have a uniform weight across the whole area at different times; rather, it indicates only the weight of a risk for a particular risk cell during a specific period. The overall score of the multi-hazard map is calculated as in Eq (2).

$$P_k = \sum_{j=1}^{n} \partial_{kj} P_{kj} \tag{2}$$

where P_k represents the risk probability of the k-th risk cell, P_{kj} represents the probability of the j-th risk in the k-th risk cell, ∂_{kj} represents the weight of the j-th risk in the k-th risk cell, and n stands for the number of haz-

ards, with $n = 3$.

2.3.3 Landscape ecological index calculation

Different ecosystems represented by different land cover types own different positions, structures, and functions in the region. The different vulnerabilities of each ecosystem will lead to different responses to the same external disturbances. According to the existing researches (Liu and Li, 2018; Zhang et al., 2018), the landscape ecological index can be regarded as a functional expression to explore the vulnerabilities of various ecosystems. Furthermore, it can reflect the degree of human disturbance that different landscapes may suffer and the relationship between landscape patterns and ecological risks. It is expressed by a landscape disturbance index (E_i) and a landscape fragility index (F_i).

The landscape disturbance index (E_i) indicates the degree of human disturbance to a specific type of landscape, as expressed in Equation (3):

$$E_i = aC_i + bS_i + cD_i \tag{3}$$

where C_i represents landscape fragmentation of the i-type landscape, which refers to the structural complexity of the landscape space, the fragmentation degree of the landscape distribution, and the degree of human interference; S_i means landscape segmentation, which reflects the regional distribution characteristics of the i-type landscape; and D_i represents the reciprocal of the perimeter-area fractal dimension and reflects the complexity of the geometry of the i-type landscape. All the three landscape indices above are calculated by using Fragstats 4.2. a, b and c represent the weights of the three landscape indices, which are assigned 0.5, 0.3 and 0.2, respectively, according to related research results (Fu and Xu, 2001; Liu and Li, 2018; Zhang et al., 2018).

The landscape fragility index (F_i) indicates the resistance ability of a specific landscape type to external disturbance. The AHP mentioned above is used to determine the landscape fragility index (F_i) of water, forest, buildings, and farmland. Moreover, the value of the matrix is determined by the order of their landscape fragility indexes F_i, with water > farmland > forest > buildings, and their F_i values are 0.4642, 0.2544, 0.1839 and 0.0975, respectively.

Therefore, the landscape ecological index of each landscape (R_i) and of each risk cell (D_k) can be constructed by Eqs. (4–5).

$$R_i = E_i \times F_i \tag{4}$$

$$D_k = \sum_{i=1}^{N} \frac{A_i}{A} R_i \tag{5}$$

where A_i and A represent the total area of the i-type landscape and the entire study area, respectively; and N stands for the number of land cover types, with $N = 4$.

2.3.4 Ecological risk assessment

After the calculation of risk probability (P_k) and the landscape ecological index (D_k), each risk cell will have a comprehensive ecological risk value, as expressed by Eq. (6):

$$R_k = P_k \times D_k \tag{6}$$

To intuitively and numerically compare the ecological risks of Huangshan Mountain in 1984, 1990, 2000, 2010 and 2019, the ecological risk index (ERI) is calculated as follows:

$$ERI = \sum_{k=1}^{K} \frac{A_k}{A} R_k \tag{7}$$

where K represents the number of risk cells, with $K = 719$; and A_k represents the area of the k-th risk cell.

3 Results

3.1 Land cover and landscape change

3.1.1 Land cover change

The land cover of Huangshan Mountain is shown in Figs. 3 and 4. Over the 35 yr, different land cover types in Huangshan Mountain had undergone different changes. As the primary land cover type, forest covers more than 90% of the area of Huangshan Mountain. In 1990, the area covered by forest was 145.37 km^2 (90.52%), reaching an all-time low. Since then, this area has started to recover gradually, and in 2019, it was more than in 1984, with a difference of 0.07 km^2. The water area had decreased between 1984 and 2019, with a total dwindling of 1.58 km^2. The area of farmland had increased sharply by 5.7% (approximately 9.08 km^2) since 1984, but was followed by a steady decrease from 1990 to 2010. Overall, the area of farmland had increased by 1.64 km^2. The changes of the building areas were more complex and frequent than the other three land cover types. From 1984 to 1990, the building areas declined by 1.66 km^2, followed by a dramatic rebound

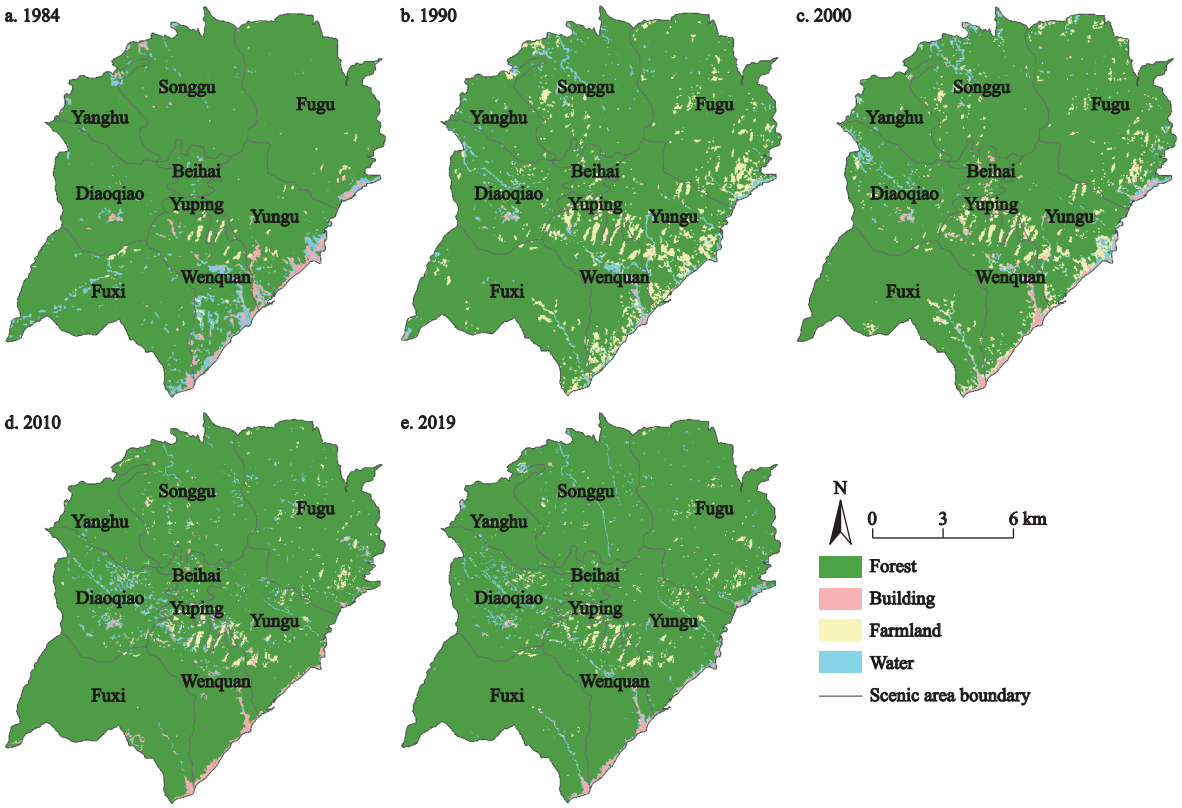

Fig. 3 Land cover maps in Huangshan Mountain, China in 1984, 1990, 2000, 2010, and 2019

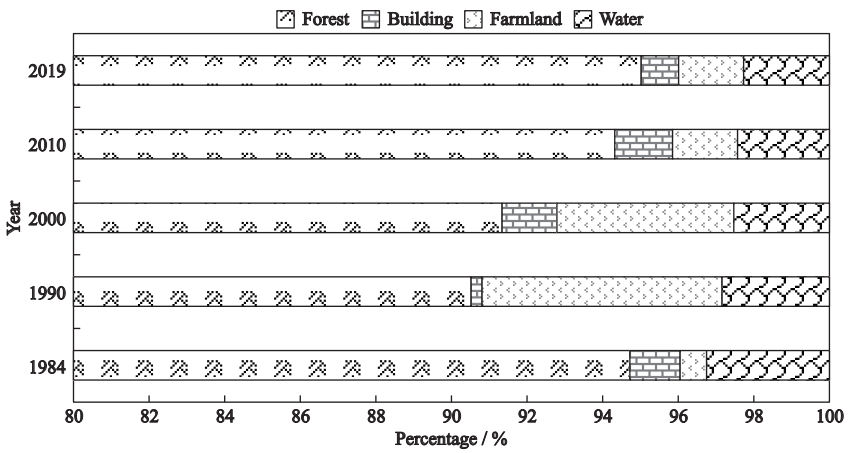

Fig. 4 Percentage changes of land cover types in Huangshan Mountain, China from 1984 to 2019

upwards, with a peak in 2010 at 2.46 km^2. And then the building areas began to decrease slowly. Overall, the building areas had decreased by 0.54 km^2.

3.1.2 Landscape pattern change

The landscape indices of the four land cover types over the period were calculated with Fragstats 4.2 (Table 2). The total number of patches in 1984, 1990, 2000, 2010 and 2019 was 869, 1249, 1550, 1444 and 1246, respectively. It can be seen that the number in 2019 increased by approximately 43.4% compared to that in 1984.

As the primary land cover type in Huangshan Mountain, the forest had the smallest C_i. Buildings and farmland showed higher landscape fragmentation due to their small areas and large numbers. Generally, water has the characteristics of aggregating in space, so its fragmentation would be small. However, water in Huangshan Mountain had the highest C_i, mainly because the water in Huangshan Mountain was blocked by tall trees and appeared in the form of mixed pixels on the images, resulting in a fragmented classification result. In addition

Table 2 Landscape indices of different land cover types in Huangshan Mountain

Land cover types	Year	Number of patches	Landscape fragmentation (C_i)	Landscape segmentation (S_i)	Landscape dominance (D_i)	Landscape disturbance (E_i)	Landscape fragility (F_i)	Landscape ecological index (R_i)
Forest	1984	176	0.0047	0.0025	1.0000	0.2031	0.1839	0.0521
	1990	52	0.0005	0.0004	0.9192	0.1843		0.0402
	2000	37	0.0000	0.0000	0.9174	0.1835		0.0397
	2010	60	0.0007	0.0005	0.9476	0.1901		0.0439
	2019	50	0.0004	0.0003	0.9509	0.1905		0.0441
Building	1984	168	0.2826	0.2239	0.0962	0.2277	0.0975	0.0000
	1990	79	0.8618	1.0000	0.0000	0.7309		0.1689
	2000	210	0.4673	0.3316	0.0862	0.3504		0.0412
	2010	272	0.5711	0.3561	0.1169	0.4157		0.0631
	2019	191	0.6189	0.4611	0.0801	0.4638		0.0792
Farmland	1984	96	0.3929	0.4131	0.0339	0.3272	0.2544	0.2101
	1990	635	0.3215	0.1300	0.3555	0.2709		0.1608
	2000	700	0.4816	0.1862	0.3156	0.3598		0.2386
	2010	360	0.6736	0.3650	0.1438	0.4751		0.3396
	2019	355	0.6638	0.3622	0.1560	0.4718		0.3367
Water	1984	429	0.4456	0.2205	0.2665	0.3422	0.4642	0.4704
	1990	483	0.5486	0.2561	0.2482	0.4008		0.5639
	2000	603	0.7678	0.3211	0.2378	0.5278		0.7668
	2010	752	1.0000	0.3747	0.3066	0.6737		1.0000
	2019	650	0.9246	0.3727	0.2991	0.6339		0.9364

to forests, the C_i of farmland, buildings and water had increased significantly from 1984 to 2019, indicating that these three land cover types were significantly disturbed by human activities. Large patch areas were divided, and the number of landscape patches and C_i increased. The changing trend of S_i of each land cover type was basically the same as that of C_i. Compared with building areas and farmland, the D_i of forests and water saw few changes, indicating that these landscapes were less affected by human interference and could maintain their original natural states. The most apparent interference from human activities was observed in farmland, with D_i increasing from 0.0641 in 1984 to 0.1533 in 2019. C_i, S_i and D_i enhanced E_i, ultimately leading to an increase in ecological risks. From 1984 to 2019, R_i of Huangshan Mountain showed an upward trend for buildings, farmland, and water, but only the R_i of forest declined slightly.

3.2 Ecological risk change

The risk probability, landscape ecological loss and ecological risk of each ecological risk cell are calculated with Eqs. (2)–(7), and they are used as the attribute values of the central point of each risk cell. Then, the spatial distribution maps of risk probability, landscape ecological loss and ecological risk in Huangshan Mountain are obtained via kriging interpolation (Fig. 5). To compare the risk probabilities in different periods, the medium value of such probabilities over time (i.e., years) is calculated as the boundary value. Values above the medium are colored red, those below the medium are blue, and those equal to the medium are yellow. The same is for the landscape ecological loss. In addition, the natural breakpoint method is used to further classify the distribution map of ecological risks into five categories in ArcGIS. The redder the color in the map, the greater the ecological risk.

As shown in Fig. 5, the ecological risk of Huangshan Mountain had changed significantly from 1984 to 2019. In general, the areas in Huangshan Mountain were at low and relatively low risk levels, with the high-risk areas mainly concentrated near the border regions. In 1990, a large number of areas with relatively low ecological risks were converted to low ecological risk ones,

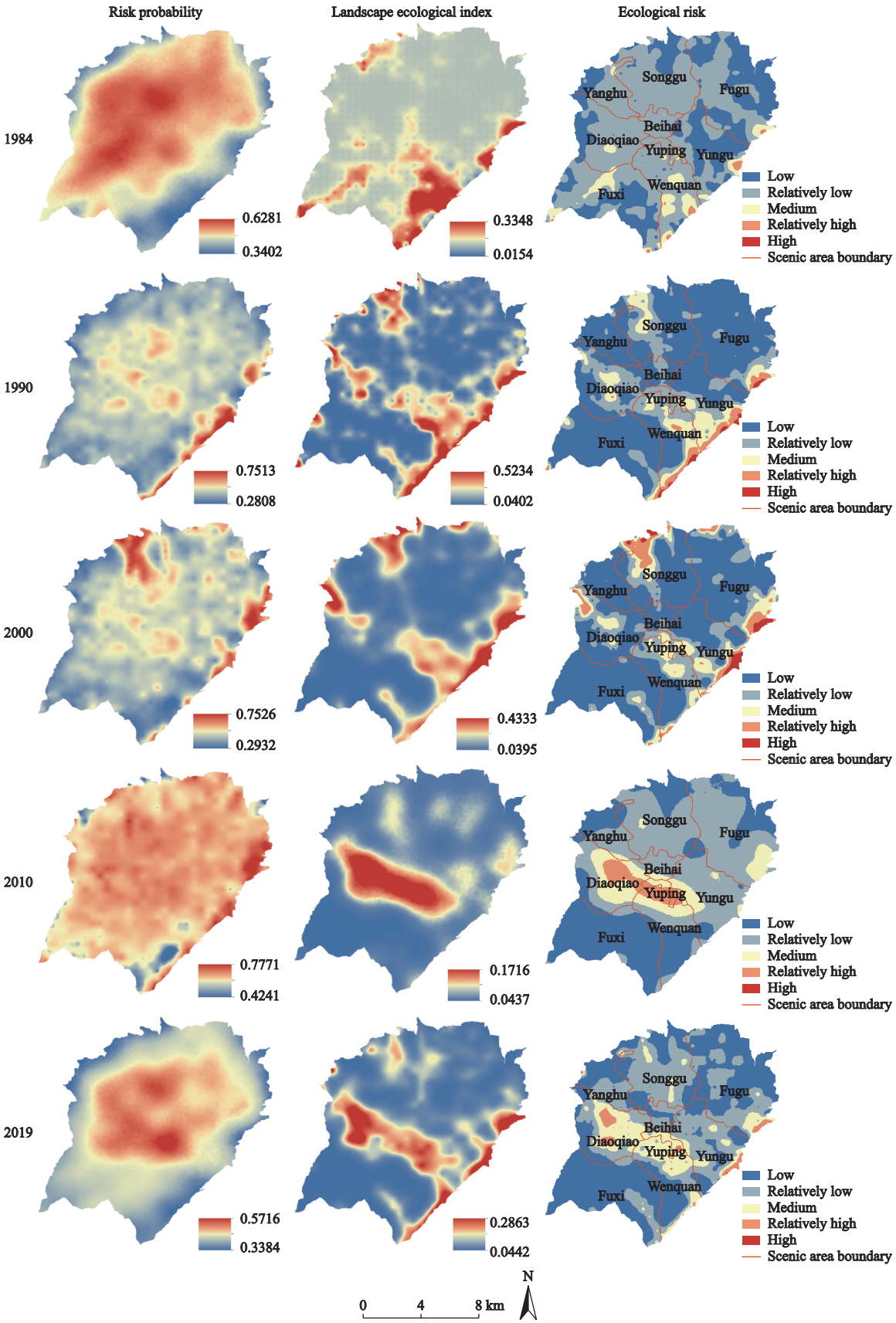

Fig. 5 Spatial distribution maps of the risk probability, landscape ecological index and ecological risk in Huangshan Mountain from 1984 to 2019

while the high ecological risk ones appeared for the first time in the southeastern and eastern border areas of Huangshan Mountain. In 2000, relatively high and high ecological risk areas emerged in the northern and western border areas. There were more high ecological risk areas in 2000 than in 1990, and the spatial distribution of ecological risks in the south-eastern region was less fragmented. The ecological risk distribution in 2010 differed significantly from that in 1984, 1990 and 2000, but was similar to that in 2019. The low-risk areas dramatically increased in 1990. Since 2010, the high ecological risk areas have disappeared.

With the help of GIS, the areas and percentages of different ecological risk levels in 1984, 1990, 2000, 2010 and 2019 could be generated (Table 3 and Fig. 6). Ecological risks in Huangshan Mountain were mainly low and relatively low. The percentages of these two kinds of areas in 1984, 1990, 2000, 2010 and 2019 were 93.97%, 87.71%, 85.66%, 84.77% and 85.53%, respectively. Although the proportion of the two kinds of areas in 1984 accounted for the most significant proportion, the lowest ecological risk of Huangshan Mountain appeared in 1990. Areas with low ecological risk in 1990 were more extensive than those in 1984, when the areas in Huangshan Mountain were mainly at a relatively low ecological risk level; in contrast, in 1990, they were mainly at a low ecological risk level. The highest ecological risk of Huangshan Mountain was observed in 2010 due to the El Niño phenomenon (see the section of Discussion).

Of the five ecological risk levels, the areas with low and relatively low ecological risks showed the most dramatic changes. For example, during this period, the areas with low ecological risks first increased, then decreased, and finally went up, showing a fluctuating trend. Such areas surged from 52.44 km^2 (32.65%) in 1984 to 107.51 km^2 (66.94%) in 1990, followed by a decrease of 48.05 km^2 from 2000 to 2010 and an increase of 18.48 km^2 from 2010 to 2019. The total area with low ecological risks had increased by 25.51 km^2 during 1984-

Table 3 Areas and percentages of different ecological risk levels

Ecological risk level	1984		1990		2000		2010		2019	
	Area / km^2	Percentage / %	Area / km^2	Percentage / %	Area / km^2	Percentage / %	Area / km^2	Percentage / %	Area / km^2	Percentage / %
Low	52.44	32.65	107.51	66.94	104.97	65.36	59.46	37.03	77.95	48.54
Relatively low	98.48	61.32	33.35	20.77	32.61	20.30	76.67	47.74	59.41	36.99
Medium	8.73	5.44	14.46	9.00	14.95	9.31	17.75	11.05	20.02	12.46
Relatively high	0.95	0.59	4.21	2.62	6.01	3.74	6.71	4.18	3.21	2.00
High	0.00	0.00	1.07	0.67	2.06	1.29	0.00	0.00	0.02	0.01
ERI	0.14054		0.13102		0.14815		0.16845		0.13926	

Note: *ERI* is ecological risk index

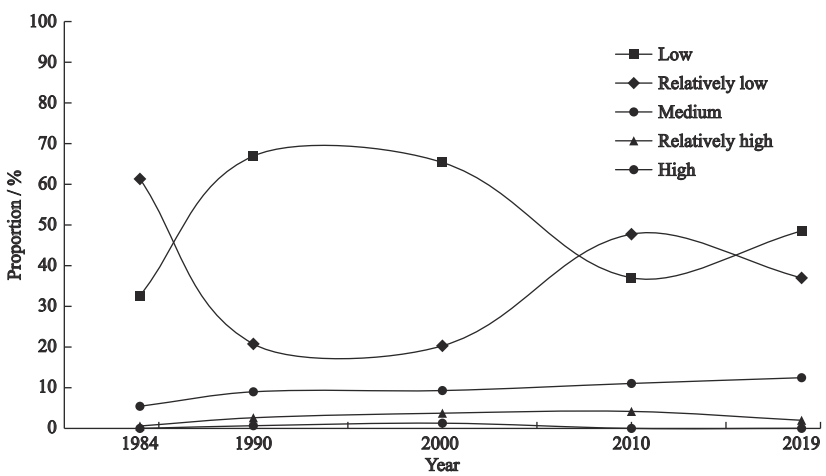

Fig. 6 Proportion changes of different ecological risk levels in Huangshan Mountain, China from 1984 to 2019

2019. The areas with relatively low ecological risks also showed a fluctuating trend, but the trend was opposite to that of low ecological risks. The total area with relatively low ecological risks had declined by 39.07 km^2 during 1984–2019. The areas at the medium ecological risk level had gradually increased over time by 11.28 km^2 from 1984 to 2019. The areas with high and relatively high ecological risks did not change much. In conclusion, the land at low and relatively low ecological risk levels was dominant in Huangshan Mountain. During the 35 yr, the size of the five ecological risk levels was diminished in the following sequence: relatively low > low > medium > relatively high > high.

4 Discussion

Obvious variations from 1984 to 2019 in terms of land cover and ecological risk are identified. From 1984 to 1990, the conversion of a large amount of forest to farmland led to a significant increase in the area of farmland. Another reason for the largest size of farmland in 1990 may lie in the demolition of a large number of buildings in Tangkou Town in the southeast region, a move that had boosted the area of wasteland, some of which may have been mistakenly classified as farmland. There was a rapid tourism development in Huangshan Mountain during 1990−2000 after the reform and opening up. Most of the infrastructure in Huangshan Mountain was also constructed in the 1990s, particularly in Tangkou Town in the southeastern region. The building areas increased substantially and reached a maximum during this period. In addition, after the Huangshan Mountain Scenic Area was included in the 'List of World Cultural and Natural Heritage' by UNESCO in 1990, the forest in Huangshan Mountain began to be effectively protected, and the destroyed forests began to recover. Since the 21st century, the government has formally launched a plan to return the farmland to the forest; later, the Yungu ropeway was built up in 2006. These measures further facilitated the restoration of the destroyed forests, such as those in the north-eastern region. Additionally, accommodation facilities within the scenic area began to move out, with buildings gradually becoming concentrated in the periphery of the scenic area. As a result, a significant increase in the forest area was delivered in Huangshan Mountain between 2000 and 2010. A large amount of water in the west region (Fig. 3d) may be related to the 2008 snow disaster when snow piled up on top of the high mountains. The removal of scenic accommodation facilities during 2010–2019 narrowed down the built-up area. Since 2010, Huangshan Mountain's land cover has remained stable.

Analyses of changes in ecological risk require the consideration of both risk probability and landscape ecological risk. For example, Huangshan Mountain was mainly at relatively low ecological risk levels in 1984 may be due to the inconsistency between the distribution of the risk probability and the landscape ecological index. Specifically, most areas of Huangshan Mountain stood at medium or high-risk probabilities, except for some areas in the southeastern region, and the areas with a high landscape ecological index were mainly concentrated in the southeast region. This phenomenon may be related to village clustering at that time. Later, from 1984 to 1990, many buildings in Tangkou Town in the southeastern region were demolished, so much wasteland appeared there. In other words, the risk probability there became high because the forest area was reduced and the vegetation was sparse due to human activities. Moreover, the distributions of both the risk probability and the landscape ecological index became consistent, that is, high-risk probabilities multiplied by high landscape ecological indices yielded high ecological risks. For example, the south-eastern fringe area became a high ecological risk area in 1990. In contrast, low risk probabilities multiplied by low landscape ecological indices yielded low ecological risks. For example, the low ecological risk area in the central region in 1984 had turned into a relatively low ecological area in 1990. As mentioned above, most of the infrastructural development in Huangshan Mountain was completed during 1990–2000. Furthermore, the Yuping and Taiping ropeways were also constructed during this period, with the latter connecting Beihai and Yuping. As a result, more high ecological risk areas emerged in 2000 than in 1990. In contrast, the remarkable increase in forest areas in the southeastern and eastern parts of Huangshan Mountain changed them from high ecological risk areas to medium and relatively low ones. However, rarely seen snow disasters in 2008 and Typhoon Morakot in 2009 had all caused changes in the natural environment (Hu et al., 2013). In addition, drought, one of the three major hazards in Huangshan

Mountain, was significantly driven by the El Niño phenomenon in 2010. All these disasters aggravated the risk probability in 2010. Furthermore, the 2008 snow disaster caused a massive amount of snow to accumulate on the top of the mountain. Therefore, in the land cover map of 2010, a large body of water with high landscape ecological loss appeared in the central part. As a result, the risk probability, landscape ecological index and ecological risk in 2010 differed from the other four yr in terms of spatial distribution. Later, in 2012, the government proposed a plan for ecological construction. The areas of buildings had fallen by 1/3, and the areas of forests had increased. It is worth noting that the maximum risk probability of Huangshan Mountain in 2019 was 0.5716, lower than that in the other four years. Therefore, the distribution of ecological risks showed a more significant relationship with the landscape ecological index in 2019 than in other yr. The high values of the landscape ecological index were mainly concentrated in the middle and southeast regions, and the distribution of the middle and relatively high ecological risk areas was basically the same. In 2019, high-risk areas almost disappeared in Huangshan Mountain. However, there was a transformation of low ecological risk areas into relatively low ones, and some high ecological risk areas appeared in Diaoqiao.

Based on the analyses above, it can be concluded that changes in ecological risks are closely related to land cover changes and natural disasters. Even though major natural disasters may have affected the ecological risk distribution in the whole region, changes in land cover caused by human activities would drive a shift in the levels of ecological risks in some areas. Take Fugu as an example: the change in the ecological risk level of Fugu is inseparable from its development. The construction of Fugu in 1990 led to an increase in its ecological risk level. The year 2010 saw a point for the ecological risk to start recovering. Therefore, it is necessary to construct tourist facilities and villages according to relevant plans. The land cover should be planned as a whole, and the construction layout should be optimized to contain the ecological risk within a controllable range. In general, areas with greater anthropogenic disturbance would encounter more ecological risks, such as Yuping. It is the essence of Huangshan Mountain and a must-visit attraction for tourists, with a high utilization rate of tourism and great interference from tourists. As a result, Yuping has seen high landscape ecological losses and ecological risks. For such scenic spots, regular rotation is a feasible protective measure.

Nevertheless, this study has some limitations that must be resolved in future research. First, it is important to solve the problem of how to establish an optimal scale for ecological risk assessment models. Some comparison tests can be set up to determine the optimal scale by comparing the results of ecological risk assessments at different scales. Second, some data about human activity trajectories, such as scenic roads, ropeways, POI locations and historical events (such as historical registries of fires), can be explored in further studies. Then, it will be possible to introduce more factors in calculating risk probability and analyze some other risks, e.g., fires and air pollution. Several studies have also demonstrated that the invasive species of pine nematodes is moving close to Huangshan Mountain. So, vegetation type data and high-resolution UAV images are needed to pinpoint the geographic location of diseased pine trees.

5 Conclusions

Both anthropogenic and natural hazards can provoke equal or different participation in WHS damage. This study considers both the natural disasters and human activities, and examines the spatial and temporal changes in ecological risk in Huangshan Mountain from 1984 to 2019. For natural hazards, this study combines the drought, erosion, and geological disaster assessment maps into one to generate the overall risk probability. Ecological disturbances to Huangshan Mountain caused by human activities are measured by the landscape ecological index.

The analysis of land cover and landscape change shows that the area of four land cover types, namely, water, forest, building, and farmland, fluctuated over the 35 yr in Huangshan Mountain, with the primary land cover type being forest. From 1984 to 2019, only the landscape ecological index of forest declined slightly, while those of the other three land cover types showed an upward trend. The analysis of ecological risk reveals that over 80% of the areas in Huangshan Mountain was low or relatively low risk, and the high ecological risk areas were mainly concentrated in the border areas, with the lowest and highest *ERI*s in 1990 and 2010, respect-

ively. In addition, from 1984 to 2019, the five ecological risk areas decreased in the following sequence: relatively low > low > medium > relatively high > high. The areas of relatively high ecological risk and those of relatively low ecological risks shifted in opposite directions, especially after 1990.

Risk preparedness and prevention are essential for the sustainable development of Huangshan Mountain. The spatial distribution map of ecological risks presented in this study can be regarded as a road map for developing proposals and adopting measures to protect and/or restore WHS. This study also provides important insights and information for policy-makers, planners and engineers. Additionally, the model developed in this study based on RS and GIS can be modified and applied to other WHSs.

References

Accardo G, Giani E, Giovagnoli A, 2003. The risk map of Italian cultural heritage. *Journal of Architectural Conservation*, 9(2): 41–57. doi: 10.1080/13556207.2003.10785342

Agapiou A, Lysandrou V, Alexakis D D et al., 2015. Cultural heritage management and monitoring using remote sensing data and GIS: the case study of Paphos area, Cyprus. *Computers, Environment and Urban Systems*, 54: 230–239. doi: 10.1016/j.compenvurbsys.2015.09.003

Agapiou A, Lysandrou V, Themistocleous K et al., 2016. Risk assessment of cultural heritage sites clusters using satellite imagery and GIS: the case study of Paphos District, Cyprus. *Natural Hazards*, 83: 5–20. doi: 10.1007/s11069-016-2211-6

Aleotti P, Chowdhury R, 1999. Landslide hazard assessment: summary review and new perspectives. *Bulletin of Engineering Geology and the Environment*, 58: 21–44. doi: 10.1007/s100640050066

Alexakis D D, Agapiou A, Themistocleous K et al., 2013. Natural and human hazard assessment of the archaeological sites of Paphos area (Cyprus) with the use of remote sensing and GIS. *Bulletin of the geological Society of Greec*, 47(3): 1448–1457. doi: 10.12681/bgsg.10983

Alexakis D, Sarris A, 2010. Environmental and human risk assessment of the prehistoric and historic archaeological sites of Western Crete (Greece) with the use of GIS, remote sensing, fuzzy logic and neural networks. In: Ioannides M et al. (eds.). *Digital Heritage*, Berlin: Springer, 332–342.

Ali S, Tong D, Xu Z et al., 2019. Characterization of drought monitoring events through MODIS- and TRMM-based DSI and TVDI over South Asia during 2001–2017. *Environmental Science and Pollution Research*, 26(32): 33568–33581. doi: 10.1007/s11356-019-06500-4

Assimakopoulos J H, Kalivas D P, Kollias V J, 2003. A GIS-based fuzzy classification for mapping the agricultural soils for N-fertilizers use. *Science of the Total Environment*, 309(1-3): 19–33. doi: 10.1016/S0048-9697(03)00055-X

Bathrellos G D, Skilodimou H D, Chousiantis K et al., 2017. Suitability estimation for urban development using multi-hazard assessment map. *Science of the Total Environment*, 575: 119–134. doi: 10.1016/j.scitotenv.2016.10.025

Belal A A, El-ramady H R, Mohamed E S et al., 2014. Drought risk assessment using remote sensing and GIS techniques. *Arabian Journal of Geosciences*, 7(1): 35–53. doi: 10.1007/s12517-012-0707-2

Cheng Jingjing, 2010. Climate resources for tourism in Hunagshan Scenic Area: analysis and exploitation. *Journal of Huangshan University*, 12(1): 42–45. (in Chinese)

Crippa C, Granata R, Margottini C et al., 2013. Afghanistan, Buddhas of Bamiyan: emergency consolidation of the cliffs and niches. In: Bilotta E et al. (eds.). *Geotechnical Engineering for the Preservation of Monuments and Historic Sites*. New York: CPC Press, 279−288

Du L, Song N P, Liu K et al., 2017. Comparison of two simulation methods of the temperature vegetation dryness index (TVDI) for drought monitoring in semi-arid regions of China. *Remote Sensing*, 9(2): 177. doi: 10.3390/rs9020177

Fu Zaiyi, XU Xuegong, 2001. Regional ecological risk assessment. *Advances in Earth Sciences*, 16(2): 267–271. (in Chinese)

Ghosh A, Kar S K, 2018. Application of analytical hierarchy process (AHP) for flood risk assessment: a case study in Malda district of West Bengal, India. *Natural Hazards*, 94: 349–368. doi: 10.1007/s11069-018-3392-y

Gong Jie, Lu Lin, Jin Xiulong et al., 2009. Impacts of tourist disturbance on plant communities and soil properties in Huangshan Mountain scenic area. *Acta Ecologica Sinica*, 29(5): 2239–2251. (in Chinese)

Guan Caihong, Hu Wei, Cheng Wenlian et al., 2005. Analysis on current situation of ecological security in Huangshan Scenic Spot. *Journal of Safety and Environment*, 3: 54–56. (in Chinese)

Hong H, Pradhan B, Xu C et al., 2015. Spatial prediction of landslide hazard at the Yihuang area (China) using two-class kernel logistic regression, alternating decision tree and support vector machines. *Catena*, 133: 266–281. doi: 10.1016/j.catena.2015.05.019

Hu Shanfeng, Wang Jinlian, Zhou Chenfeng et al., 2013. Research on the risk assessment and prevent to collapse disaster in Huangshan scenic area. *Geographical Research*, 10: 1814–1823. (in Chinese)

Huang Chenglin, 1992. Study on control measures of tourist overload during peak season of Huangshan Mountain. *Economic*

Geography, 3: 85–89, 92. (in Chinese)

Hunsaker C T, Graham R L, Suter G W et al., 1990. Assessing ecological risk on a regional scale. *Environmental Management*, 14(3): 325–332. doi: 10.1007/BF02394200

Isceah I, Zhan G, Araoz G et al., 2010. China: heritage in the aftermath of the Sichuan Earthquake/Kashgar, Heritage at risk. *Heritage at Risk*, 46–51. doi: 10.11588/hr.2010.0.19856

Joppa L N, O'Connor B, Visconti P et al., 2016. Filling in biodiversity threat gaps. *Science*, 352(6284): 416–418. doi: 10.1126/science.aaf3565

Kayastha P, Dhital M R, Smedt DE F, 2013. Application of the analytical hierarchy process (AHP) for landslide susceptibility mapping: a case study from the Tinau watershed, west Nepal. *Computers & Geosciences*, 52: 398–408. doi: 10.1016/j.cageo.2012.11.003

Levin N, Ali S, Crandall D et al., 2019. World Heritage in danger: Big data and remote sensing can help protect sites in conflict zones. *Global environmental change*, 55: 97–104. doi: 10.1016/j.gloenvcha.2019.02.001

Li J, Pu R, Gong H et al., 2017. Evolution characteristics of landscape ecological risk patterns in coastal zones in Zhejiang Province, China. *Sustainability*, 9(4): 584. doi: 10.3390/su9040584

Liang Taiqin, 1993. On the development of Huangshan mountain scenic areas and the conservation strategies of eco-environment. *Resources Science*, 4: 66–73. (in Chinese)

Liu J, Xu Z, Chen F et al., 2019. Flood hazard mapping and assessment on the Angkor world heritage site, Cambodia. *Remote Sensing*, 11(1): 98. doi: 10.3390/rs11010098

Liu Y, Li J, 2018. Evolution of landscape ecological risk at the optimal scale: A case study of the open coastal wetlands in Jiangsu, China. *International Journal of Environmental Research and Public Health*, 15(8): 1691. doi: 10.3390/ijerph15081691

Lyu H, Shen J S, Arulrajah A, 2018. Assessment of geohazards and preventative countermeasures using AHP incorporated with GIS in Lanzhou, China. *Sustainability*, 10(2): 304. doi: 10.3390/su10020304

Ma Bingran, Zeng Wweihua, Xie Yuxi, 2019. The functional zoning method for natural parks: a case study of Huangshan Scenic area. *Acta Ecologica Sinica*, 39(22): 8286–8298. (in Chinese)

Mecocci A, Abrardo A, 2014. Monitoring architectural heritage by wireless sensors networks: San Gimignano—A case study. *Sensors*, 14(1): 770–778. doi: 10.3390/s140100770

Ministry of Land and Resources of the People ’s Republic of China, 2017. *Current Land Use Classification: GB/T* 21010–2017. Beijing: Ministry of Land and Resources of the People’s Republic of China. 1−6. (in Chinese)

Ministry of Water Resources of the People’s Republic of China, 2008. *Standards for Classification and Gradtion of Soil Erosion: SL* 190−2007. Beijing: Ministry of Water Resources of the People’s Republic of China, 8−14. (in Chinese)

Murray N J, Keith D A, Bland L M et al., 2018. The role of satellite remote sensing in structured ecosystem risk assessment. *Science of the Total Environment*, 619: 249–257. doi: 10.1016/j.scitotenv.2017.11.034

Norton S B, Rodier D J, Schalie W H et al., 1992. A framework for ecological risk assessment at the EPA. *Environmental toxicology and chemistry*, 11(12): 1663–1672. doi: 10.1002/etc.5620111202

Pandey A, Mathur A, Mishra S K et al., 2009. Soil erosion modeling of a Himalayan watershed using RS and GIS. *Environmental Earth Sciences*, 59(2): 399–410. doi: 10.1007/s12665-009-0038-0

Papadopoulou-Vrynioti K, Bathrellos G D, Skilodimou H D et al., 2013. Karst collapse susceptibility mapping considering peak ground acceleration in a rapidly growing urban area. *Engineering Geology*, 158: 77–88. doi: 10.1016/j.enggeo.2013.02.009

Ryan J, Silvanto S, 2009. The World Heritage List: the making and management of a brand. *Place Branding and Public Diplomacy*, 5: 290–300. doi: 10.1057/pb.2009.21

Sandlot I, Rasmussen K, Andersen J, 2002. A simple interpretation of the surface temperature/vegetation index space for assessment of surface moisture status. *Remote Sensing of Environment*, 79(2–3): 213–224. doi: 10.1016/S0034-4257(01)00274-7

Siddayao G P, Valdez S E, Fernandez P L, 2014. Analytic hierarchy process (AHP) in spatial modeling for floodplain risk assessment. *International Journal of Machine Learning and Computing*, 4(5): 450. doi: 10.7763/IJMLC.2014.V4.453

Skilodimou H D, Bathrellos G D, Chousiantis K et al., 2019. Multi-hazard assessment modeling via multi-criteria analysis and GIS: a case study. *Environmental Earth Sciences*, 78(2): 1–21. doi: 10.1007/s12665-018-8003-4

Sugio K, 2015. Large-scale disasters on world heritage and cultural heritage in Japan: significant impacts and sustainable management cases. *Landscape Research*, 40(6): 748–758. doi: 10.1080/01426397.2015.1057806

Turner M G, Gardner R H, O’neill R V *et al.* , 2001. *Landscape Ecology in Theory and Practice*. Springer New York. USA: Springer Verlag, 401.

UNESCO, 2019. *World Heritage Centre Operational Guidelines for the Implementation of the World Heritage Convention*. Paris: UNESCO World Heritage Centre, 45–53.

Wang Peiyu, Yan Lu, Ren Chunyang et al., 2021. Spatio-temporal characteristics of Internet attention and tourist flow: a case study of Huangshan City, Anhui Province. *Hebei Enterprise*, 10: 95–98. (in Chinese)

Wang Qun, Lu Lin, Yang Xingzhu, 2014. Security assessment of

water resources system for mountain resorts based on set pair analysis: a case study of Huangshan. *Geographical Research*, 33(6): 1059–1072. (in Chinese)

Yan C, Morrison A M, 2008. The influence of visitors' awareness of world heritage listings: a case study of Huangshan, Xidi and Hongcun in southern Anhui, China. *Journal of Heritage Tourism*, 2(3): 184–195. doi: 10.2167/jht059.0

Yang, Cizhong, 2014. Sensitivity Analysis of Eco-geological Environment in the Huangshan Scenic Area based on '3S' Technology. Hefei: Hefei University of Technology. (in Chinese)

Zang Liping, Shan Yongxiang, Kong Xun, 2018. Application of GIS-based analytic hierarchy process in geological hazards assessment in Tongde Count. *Journal of Qinghai University*, 36(6): 58–64. (in Chinese)

Zhang F, Yushanjiang A, Wang D, 2018. Ecological risk assessment due to land cover changes (LUCC) in Jinghe County, Xinjiang, China from 1990 to 2014 based on landscape patterns and spatial statistics. *Environmental Earth Sciences*, 77(13): 1–16. doi: 10.1007/s12665-018-7676-z

Zhang Shunqiang, Qing Qingtao, Hou Meiting et al., 2007. Remote sensing and impact estimation for Sichuan hot-drought based on temperature vegetation dryness index. *Transactions of the Chinese Society of Agricultural Engineering*, 9: 141–146, 284. (in Chinese)

Zhang W, Chang W J, Zhu Z C et al., 2020. Landscape ecological risk assessment of Chinese coastal cities based on land use change. *Applied Geography*, 117: 102174. doi: 10.1016/j.apgeog.2020.102174

Zhang Yazhou, Xie Xiaoping, 2015. Ecological risk assessment of Nansi Lake based on RS and GIS. *Journal of Ecology*, 35(5): 1371–1377. (in Chinese)

Zhou Haohao, Feng Hengdong, 2018. Based on remote sensing and geographic information system in dynamic monitoring and evaluation of ecological environment for Hunchun City. *Journal of Yanbian University* **(***Natural Science***)**, 44(2): 183–188. (in Chinese)